processes

MDPI

Article

Solubility Measurement and Correlation of Cis-1,1,1,4,4,4-Hexafluoro-2-butene in Dipentaerythritol Hexaheptanoate and Dipentaerythritol Isononanoate from 293.15 K to 343.15 K

Cheng Lu, Wenzhe Dang and Xiaopo Wang *

Key Laboratory of Thermo-Fluid Science and Engineering, Ministry of Education, School of Energy and Power Engineering, Xi'an Jiaotong University, Xi'an 710049, China
* Correspondence: wangxp@xjtu.edu.cn; Tel.: +86-29-82668210

Abstract

Cis-1,1,1,4,4,4-hexafluoro-2-butene (R1336mzz(Z)) is a highly promising alternative refrigerant, particularly in heat pumps with large temperature lifts. To meet the superheat requirement of R1336mzz(Z), the heat pump system typically requires the installation of an internal heat exchanger, which renders system performance more sensitive to the solubility of the refrigerant in lubricant. Dipentaerythritol ester (DiPEC) is one of the main components of POE lubricants. In this study, the solubilities of R1336mzz(Z) in two DiPECs, dipentaerythritol hexaheptanoate (DiPEC7) and dipentaerythritol isononanoate (DiPEiC9), were measured in the temperature range of 293.15 K–343.15 K. The solubility data were correlated using the non-random two-liquid (NRTL) model; the average absolute relative deviation between this work and values from NRTL model is lower than 2%. In addition, the Henry's constants of R1336mzz(Z) in DiPEC7 and DiPEiC9 were calculated, and the dissolution potential was compared. Moreover, the mixing thermodynamic properties (such as mixing enthalpy change, mixing entropy change, and mixing Gibbs free energy change) of R1336mzz(Z) dissolving in DiPECs were analyzed.

Keywords: R1336mzz(Z); DiPEC7; DiPEiC9; solubility; NRTL model; Raoult's Law; Henry's Constant

check for updates

Academic Editor: Andrey Voshkin

Received: 22 October 2025
Revised: 12 November 2025
Accepted: 14 November 2025
Published: 17 November 2025

Citation: Lu, C.; Dang, W.; Wang, X. Solubility Measurement and Correlation of Cis-1,1,1,4,4,4-Hexafluoro-2-butene in Dipentaerythritol Hexaheptanoate and Dipentaerythritol Isononanoate from 293.15 K to 343.15 K. *Processes* **2025**, *13*, 3704. https://doi.org/10.3390/pr13113704

Copyright: © 2025 by the authors. Licensee MDPI, Basel, Switzerland. This article is an open access article distributed under the terms and conditions of the Creative Commons Attribution (CC BY) license (https://creativecommons.org/licenses/by/4.0/).

1. Introduction

The Kigali Amendment to the Montreal Protocol has provided significant guidance for global environmental governance and has currently been endorsed by 197 parties. Since the amendment entered into force on 1 January 2019, the clear timetable has accelerated the phase-out of refrigerants with high global warming potential (GWP) [1–4]. In the field of industrial heat pumps, traditional refrigerants, represented by R245fa (GWP = 1030), are required to be gradually phased out due to their high environmental impact. Hydrofluoroolefin (HFO) refrigerants, relying on their low GWP, have become the primary alternative solution [5]. Among them, cis-1,1,1,4,4,4-hexafluoro-2-butene (R1336mzz(Z), GWP = 2) is a highly promising alternative refrigerant for heat pumps and organic Rankine cycles [6–8]. R1336mzz(Z) features a critical temperature of 444.5 K, which enables it to fully meet the operational requirements of high-temperature heat pumps, thus demonstrating considerable application potential in the food drying and chemical processing industries. Furthermore, its A1 safety classification and excellent high-temperature chemical stability ensure the

safety of R1336mzz(Z) in practical applications. At present, comprehensive research has been conducted on the basic thermophysical properties of R1336mzz(Z), including critical parameters [7], saturated vapor pressure [9], specific heat capacity [10], viscosity [11], and thermal conductivity [12,13].

For vapor compression heat pumps, the effect of compressor lubricants deserves attention. Elevated operating temperatures may cause lubricant carbonization or a significant decrease in viscosity. Polyol ester (POE) lubricants are suitable for high-temperature heat pumps, as their core component exhibits high thermal stability and a wide viscosity range [14]. Pentaerythritol ester (PEC) and dipentaerythritol ester (DiPEC) are the main components of POE lubricants. Generally speaking, the increase in the number of ester groups in PEC or DiPEC leads to an increase in viscosity [15]. PECs typically have a kinematic viscosity of 10–30 mPa·s at 40 °C [16], while DiPECs exceed 50 mPa·s at 40 °C [17]. The introduction of branched structures can also significantly increase the viscosity of polyol esters. As an example, the kinematic viscosity of dipentaerythritol isononanoate (one of the branched esters) at 40 °C exceeds 390 mPa·s [18,19]. Beyond the intrinsic properties of lubricants, the miscibility between R1336mzz(Z) and polyol esters is also of importance because the miscibility not only drastically alters the lubricant viscosity [20,21] but also degrades the heat transfer capability of R1336mzz(Z) [22]. In addition, understanding the solubility of R1336mzz(Z) in polyol esters enables the optimization of heat pumps. However, to the best of our knowledge, only Brocus et al. measured the solubility of R1336mzz(Z) in POE SE220 [23]; no other measurements have been reported yet.

To fill the gap, in this work, the solubility of R1336mzz(Z) in dipentaerythritol hexaheptanoate (DiPEC7) and dipentaerythritol isononanoate (DiPEiC9) was measured using the isochoric saturation method from 293.15 K to 343.15 K. Based on the solubility data, the deviations of the two mixtures from Raoult's law were calculated. The non-random two-liquid (NRTL) model was employed to calculate the mole fraction of R1336mzz(Z) in DiPECs. The mixing thermodynamic properties of the mixtures were calculated and analyzed.

2. Experimental Method

2.1. Experimental Samples

The refrigerant (R1336mzz(Z)) was provided by Honeywell, and the DiPEC7 and DiPEiC9 used in present work were supplied by MingKT Corporation. Table 1 presents the basic information of the materials. Figures 1 and 2 show the molecular structures of R1336mzz(Z) and the DiPECs.

Table 1. Basic information on the materials.

	Formula	CAS No.	Supplier	Mass Fraction Purity
R1336mzz(Z) [a]	$C_4H_2F_6$	692-49-9	Honeywell	0.999
DiPEC7 [b]	$C_{52}H_{94}O_{13}$	76939-66-7	MingKT Corporation	0.99
DiPEiC9 [c]	$C_{64}H_{118}O_{13}$	127304-08-9	MingKT Corporation	0.99

[a] cis-1,1,1,4,4,4-hexafluoro-2-butene, [b] dipentaerythritol hexaheptanoate, [c] dipentaerythritol isononanoate.

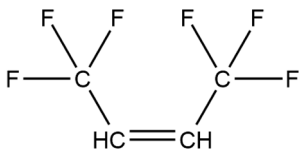

Figure 1. Molecular structure of R1336mzz(Z).

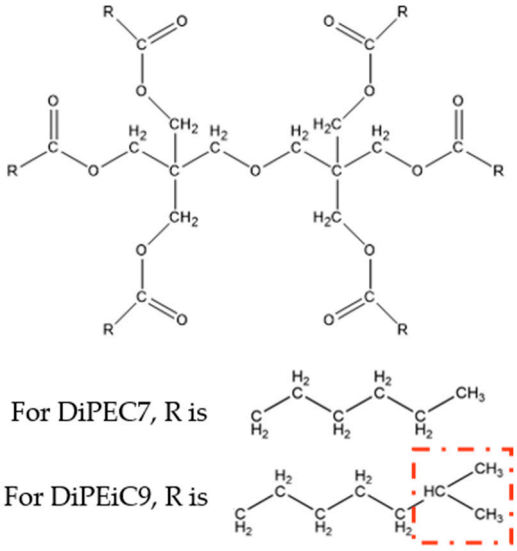

Figure 2. Molecular structures of DiPEC7 and DiPEiC9.

2.2. Experimental Setup

García et al. measured the saturated vapor pressures of DiPEC7 and DiPEiC9 [15], and their values are almost negligible compared with those of refrigerants. Therefore, the isochoric saturation method was used to measure the solubility of R1336mzz(Z) in DiPEC7 and DiPEiC9. Figure 3 presents the schematic diagram of the experimental system. As the experimental apparatus and procedures have been described in detail in our previous reports [24,25], only a brief introduction is provided here.

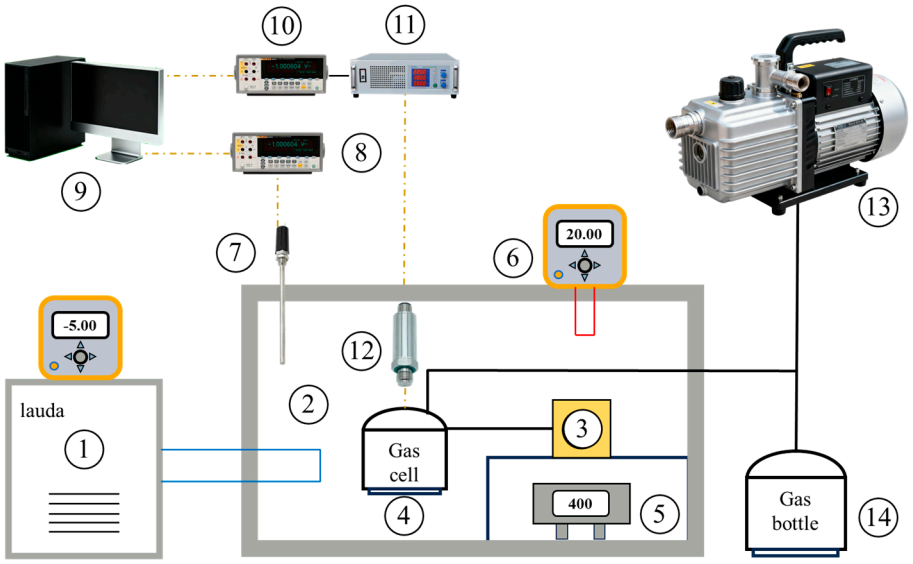

Figure 3. Schematic diagram of the solubility experimental system. ① Cooling bath, ② thermostat bath, ③ equilibrium cell, ④ gas cell, ⑤ magnetic stirrer, ⑥ temperature controller, ⑦ thermometer, ⑧ digital multimeter, ⑨ data acquisition computer, ⑩ multimeter, ⑪ DC power, ⑫ pressure transducer, ⑬ vacuum pump, ⑭ gas bottle.

Preceding the experiment, the refrigerant R1336mzz(Z) was introduced into the gas cell. A precision balance (Mettler Toledo, Zurich, Switzerland; Model: ME204, accuracy: ±0.0002 g) was used to weigh the DiPEC lubricant, which was then placed into the equilibrium cell. The calibrated volumes of the gas cell and equilibrium cell were determined to be 103.60 ± 0.02 cm^3 and 33.37 ± 0.02 cm^3, respectively. Upon opening the valve connecting the gas cell and equilibrium cell, the R1336mzz(Z) flowed into the equilibrium

cell and dissolved in the lubricant. The system pressure exhibited a gradual decrease due to gas dissolution, and the pressure drop was utilized to compute the solubility of the R1336mzz(Z) in DiPECs. Temperature measurements were performed with a platinum resistance thermometer (Fluke, Everett, USA; Model: 5608,accuracy: 0.01 K), while pressure was measured using a pressure transducer (Keller, Winterthur, Switzerland; Model: 33X, accuracy: 0.03% FS, range: 0–3 MPa). In this work, the expanded uncertainties for temperature and pressure measurements were less than 0.02 K and 2.0 kPa (k = 2), respectively.

The solubility of R1336mzz(Z) in DiPECs is expressed in two forms in this work: mole fraction (x_1) and mass fraction (w_1). Equations (1) and (2) are used to calculate x_1 and w_1, respectively:

$$x_1 = \frac{n_1}{n_1 + n_2} \tag{1}$$

$$w_1 = \frac{n_1 \cdot M_1}{n_1 \cdot M_1 + n_2 \cdot M_2} \tag{2}$$

In all formulas used in this work, the subscripts "1" and "2" denote R1336mzz(Z) and DiPECs, respectively. n and M represent the number of moles and molar mass. n_2 can be directly calculated using $n_2 = m_2/M_2$, while n_1 is obtained by solving Equations (3) and (4) simultaneously:

$$n_1 = n_1^0 - n_1^1 = \rho_1^0 V_{gc} - \rho_1^1 \left(V_{gc} + V_{ec} - V_{1,liquid} - V_2 \right) \tag{3}$$

and

$$V_{1,liquid} = n_1 / \rho_{1,liquid}^1 \tag{4}$$

In Equations (3) and (4), superscripts "0" and "1" denote the initial and equilibrium states. V_{gc} and V_{ec} represent the volumes of the gas cell and the equilibrium cell, respectively. V_2 is the volume of the DiPECs and is calculated by $V_2 = m_2/\rho_2$; ρ_2 is obtained from Ref. [19]. $\rho_{1,liquid}^1$ represents the liquid density of R1336mzz(Z), which has been reported by Sun et al. [26].

In accordance with the principle of uncertainty propagation [27], the experimental uncertainty of solubility measurement $U_{exp}(x_1)$ can be calculated. Equation (5) shows the expression for uncertainty propagation:

$$U_{exp}(x_1) = k \cdot \sqrt{\begin{array}{l} \left(\frac{\partial x_1}{\partial \rho_1^0}\right)^2 \cdot u^2(\rho_1^0) + \left(\frac{\partial x_1}{\partial \rho_1^1}\right)^2 \cdot u^2(\rho_1^1) + \left(\frac{\partial x_1}{\partial \rho_2}\right)^2 \cdot u^2(\rho_2) + \left(\frac{\partial x_1}{\partial \rho_{1,liquid}^1}\right)^2 \cdot u^2\left(\rho_{1,liquid}^1\right) \\ + \left(\frac{\partial x_1}{\partial V_{gc}}\right)^2 \cdot u^2(V_{gc}) + \left(\frac{\partial x_1}{\partial V_{ec}}\right)^2 \cdot u^2(V_{ec}) + \left(\frac{\partial x_1}{\partial m_2}\right)^2 \cdot u^2(m_2) \end{array}} \tag{5}$$

where k is the coverage factor (k = 2). Table 2 lists the uncertainty associated with each parameter in Equation (5).

Table 2. Uncertainties of various parameters.

Source of Uncertainty	Uncertainty	Source of Uncertainty	Uncertainty
$u(V_{gc})$	0.02 cm^3	$u(\rho_1^0)$	$0.005\rho_1^0$
$u(V_{ec})$	0.02 cm^3	$u(\rho_1^1)$	$0.005\rho_1^1$
$u(\rho_2)$	0.0008 g·cm^{-3}	$u(\rho_{1,liquid}^1)$	$0.005\rho_{1,liquid}^1$
$u(m_2)$	0.0002 g		

In Equation (3), the volume change of DiPECs in an equilibrium cell after absorption is only considered as the volume of dissolved saturated liquid R1336mzz(Z), and the excess molar volume (V^E) of the R1336mzz(Z)/DiPECs mixture is not included. According to the results reported by Goharshadi et al. [28] and Comuñas et al. [29], the excess molar volume

of refrigerants dissolved in organic solvents is typically less than 10 cm^3/mol. Considering the V^E, Equation (3) can be rewritten as follows:

$$n_1 = n_1^0 - n_1^1 = \rho_1^0 V_{gc} - \rho_1^1 \left(V_{gc} + V_{ec} - V_{1,liquid} - V_2 - V^E \right) \quad (6)$$

By comparing the calculated mole fraction using Equations (3) and (6), the uncertainty induced by the excess molar volume $U_{VE}(x_1)$ can be determined. Subsequently, the combined expanded uncertainty of the mole fraction $U(x_1)$ can be calculated:

$$U(x_1) = \sqrt{U_{exp}{}^2(x_1) + U_{VE}{}^2(x_1)} \quad (7)$$

Calculated results show that the values for the combined expanded relative uncertainty of the mole fraction $U_r(x_1)$ are 2.72% for the R1336mzz(Z)/DiPEC7 mixture and 2.85% for the R1336mzz(Z)/DiPEiC9 mixture, respectively.

2.3. NRTL Model

In this work, the experimental solubility data of R1336mzz(Z) in DiPEC7 and DiPEiC9 were correlated based on the non-random two-liquid (NRTL) activity coefficient model. For the studied systems, the refrigerant R1336mzz(Z) at the equilibrium state can be described by the following equation [30]:

$$E\gamma_1 x_1 p_1^s = y_1 p \quad (8)$$

where p_1^s is the vapor pressure of R1336mzz(Z), which was reported by Sacoda et al. [10]. y represents the mole fraction in gas phase. E is the enhancement factor, which is calculated using Equation (9):

$$E = \zeta_1 \frac{\varphi_1^s}{\varphi_1^v} = \frac{\varphi_1^s}{\varphi_1^v} \exp\left(\frac{p - p_1^s}{\rho_{1,liquid}^1 RT} \right) \quad (9)$$

In Equation (9), ζ_1 is the Poynting correction factor. φ_1^v and φ_1^s are the fugacity coefficients of R1336mzz(Z) at the equilibrium state and at the saturated state, which can be calculated as follows:

$$\varphi_1^v = \exp\left(\frac{B\ p}{RT} \right) \quad (10)$$

and

$$\varphi_1^s = \exp\left(\frac{B\ p_1^s}{RT} \right) \quad (11)$$

where R is the universal gas constant, with a value of 8.31446 $J \cdot mol^{-1} \cdot K^{-1}$. B is the second virial coefficient of the mixture, which is calculated as follows [31]:

$$B = y_1{}^2 B_{11} + y_2{}^2 B_{22} + 2 y_1 y_2 B_{12} \quad (12)$$

where B_{11} and B_{22} are the second virial coefficients of R1336mzz(Z) and DiPECs, respectively. B_{12} is the second virial coefficient resulting from the mixing process. Because $y_1 = 1$ and $y_2 = 0$, $B = B_{11}$. B_{11} was obtained from REFPROP 10.0 [32].

In the NRTL model, γ_1 can be calculated as follows [33]:

$$\ln \gamma_1 = x_2^2 \left\{ \tau_{21} \left[\frac{\exp(-\alpha\tau_{21})}{x_1 + x_2 \exp(-\alpha\tau_{21})} \right]^2 + \frac{\tau_{12} \exp(-\alpha\tau_{12})}{[x_2 + x_1 \exp(-\alpha\tau_{12})]^2} \right\} \quad (13)$$

In Equation (13), α is the non-randomness parameter, which is considered to be 0.2 here. τ_{12} and τ_{21} are the binary interaction parameters which are considered as a function of temperature T:

$$\tau_{12} = \tau_{12,0} + \tau_{12,1} \cdot T + \tau_{12,2} \cdot T^2 \quad (14)$$

and

$$\tau_{21} = \tau_{21,0} + \tau_{21,1} \cdot T + \tau_{21,2} \cdot T^2 \quad (15)$$

where $\tau_{12,0}$, $\tau_{12,1}$, $\tau_{12,2}$, $\tau_{21,0}$ $\tau_{21,1}$, and $\tau_{21,2}$ are the adjustable parameters and can be obtained via the regression of the experimental solubility data.

3. Experimental Results and Discussion

3.1. Experimental Data and Correlation

Tables 3 and 4 list the mole fraction (x_1) values of R1336mzz(Z) in DiPEC7 and DiPEiC9 over the temperature range of 293.15 to 343.15 K. For practical application purpose, the mass fractions (w_1) of R1336mzz(Z) in DiPECs are also given in Tables 3 and 4. Figures 4 and 5 show the effects of temperature and pressure on the mole fraction x_1. As expected, the mole fractions of R1336mzz(Z) in DiPEC7 and DiPEiC9 increase with decreasing temperature and increasing pressure.

Table 3. *p-T-x* (w) data of R1336mzz(Z) (1) in DiPEC7 (2) [a].

T (K)	p (MPa)	x_1	w_1	T (K)	p (MPa)	x_1	w_1
293.15	0.008	0.099	0.019	323.15	0.026	0.183	0.038
293.15	0.020	0.215	0.046	323.15	0.044	0.283	0.065
293.15	0.033	0.324	0.078	323.15	0.061	0.374	0.095
293.15	0.046	0.419	0.113	323.15	0.082	0.440	0.122
293.15	0.059	0.494	0.147	333.15	0.012	0.074	0.014
303.15	0.009	0.093	0.018	333.15	0.029	0.167	0.034
303.15	0.022	0.205	0.044	333.15	0.048	0.263	0.059
303.15	0.036	0.311	0.074	333.15	0.068	0.351	0.087
303.15	0.050	0.406	0.108	333.15	0.091	0.415	0.112
303.15	0.066	0.477	0.139	343.15	0.013	0.066	0.012
313.15	0.024	0.195	0.041	343.15	0.032	0.150	0.030
313.15	0.039	0.299	0.070	343.15	0.054	0.238	0.052
313.15	0.055	0.391	0.102	343.15	0.076	0.318	0.076
313.15	0.073	0.461	0.131	343.15	0.102	0.381	0.098

[a] $U(x_1)$ = 2.72%, $u(T)$ = 0.02 K, and $u(p)$ = 2.00 kPa.

Table 4. *p-T-x* (w) data of R1336mzz(Z) (1) in DiPEiC9 (2) [a].

T (K)	p (MPa)	x_1	w_1	T (K)	p (MPa)	x_1	w_1
293.15	0.010	0.105	0.017	313.15	0.073	0.504	0.132
293.15	0.024	0.243	0.046	323.15	0.013	0.089	0.014
293.15	0.037	0.353	0.075	323.15	0.030	0.206	0.037
293.15	0.050	0.457	0.112	323.15	0.047	0.311	0.063
293.15	0.059	0.536	0.147	323.15	0.065	0.412	0.095
303.15	0.010	0.099	0.016	323.15	0.081	0.484	0.123
303.15	0.026	0.231	0.043	333.15	0.013	0.085	0.014
303.15	0.040	0.340	0.072	333.15	0.033	0.190	0.034
303.15	0.054	0.444	0.107	333.15	0.052	0.290	0.058
303.15	0.066	0.521	0.140	333.15	0.090	0.460	0.113
313.15	0.012	0.095	0.015	343.15	0.058	0.264	0.051
313.15	0.028	0.220	0.040	343.15	0.080	0.358	0.077
313.15	0.043	0.328	0.068	343.15	0.101	0.428	0.101
313.15	0.059	0.430	0.101				

[a] $U(x_1)$ = 2.85%, $u(T)$ = 0.02 K, and $u(p)$ = 2.00 kPa.

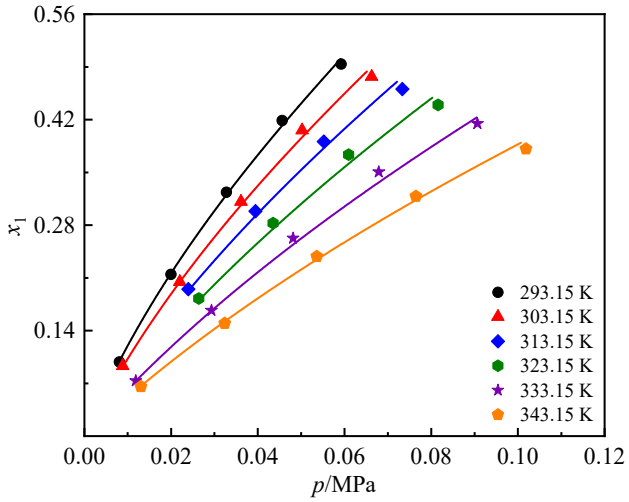

Figure 4. *p-T-x* diagram of R1336mzz(Z) in DiPEC7. The solid line represents the calculated results from the NRTL model.

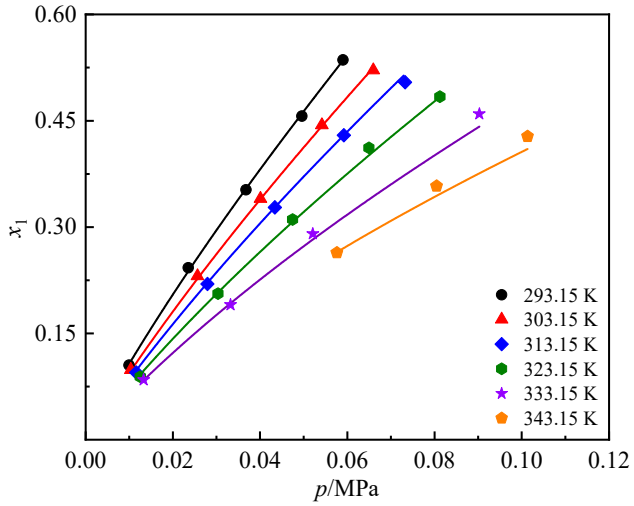

Figure 5. *p-T-x* diagram of R1336mzz(Z) in DiPEiC9. The solid line represents the calculated results from the NRTL model.

Table 5 lists the regressed parameters in the NRTL model. Figures 6 and 7 show the deviation distributions between each set of experimental data and the calculated values from the NRTL model. It is obvious that the average absolute relative deviation (AARD) and maximum absolute relative deviation (MARD) between the experimental mole fractions and the calculated values from NRTL model are 1.88% and 3.93% for R1336mzz(Z)/DiPEC7 system, and 1.46% and 4.17% for R1336mzz(Z)/DiPEiC9 system. The NRTL model can represent the experimental solubility data with good accuracy.

Table 5. Parameters in NRTL model for R1336mzz(Z)/DiPEC7 and R1336mzz(Z)/DiPEiC9 systems.

	R1336mzz(Z)/DiPEC7	**R1336mzz(Z)/DiPEiC9**
$\tau_{12,0}$	659.1357	4000.9680
$\tau_{12,1}$	−4.6958	−27.4281
$\tau_{12,2}$	0.0090	0.0490
$\tau_{21,0}$	−15.6776	−18.0989
$\tau_{21,1}$	0.0924	0.1185
$\tau_{21,2}$	−0.0001	−0.0002
$AARD/\%$ [a]	1.88	1.46
$MARD/\%$ [b]	3.93	4.17

[a] $AARD/\% = 100/n\sum_{i=1}^{n}\left(\left|x_i^{cal} - x_i^{exp}\right|/x_i^{exp}\right)$, [b] $MARD/\% = 100\max\left(\left|x_i^{cal} - x_i^{exp}\right|/x_i^{exp}\right)$.

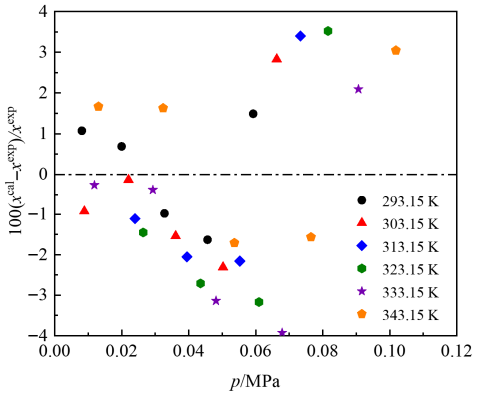

Figure 6. Deviations between experimental and calculated values for R1336mzz(Z)/DiPEC7.

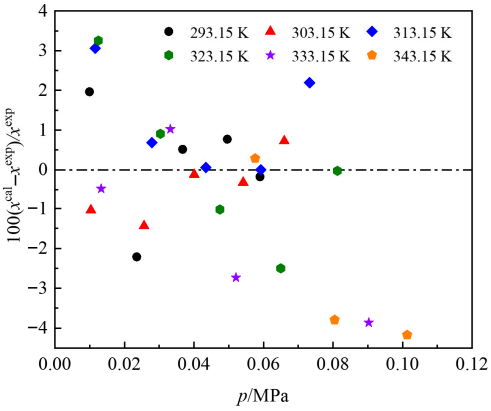

Figure 7. Deviations between experimental and calculated values for R1336mzz(Z)/DiPEiC9.

The deviation of a mixture from Raoult's law reflects the non-ideality of the solution. According to Raoult's law [34], the total vapor pressure of an ideal system can be calculated using the following equation:

$$p^* = x_1 p_1^s + x_2 p_2^s \quad (16)$$

where p^* represents the total vapor pressure of the ideal solution. p_1^s and p_2^s represent the saturated vapor pressures of R1336mzz(Z) and the DiPECs. Because the saturated vapor pressure of the DiPECs is negligible [24], $p^* = x_1 p_1^s$. The deviation between the actual pressure p and the ideal pressure p^* reflects the deviation of the R1336mzz(Z)/DiPECs system from Raoult's law, as indicated in Figures 8 and 9. As the temperature increases, the binary mixtures gradually shift from positive deviation to negative deviation from Raoult's law. This indicates that, as temperature increases, the intermolecular forces between R1336mzz(Z) and DiPECs gradually become stronger than those among R1336mzz(Z) molecules. The conclusion can provide support for analyzing the solubility at higher temperatures.

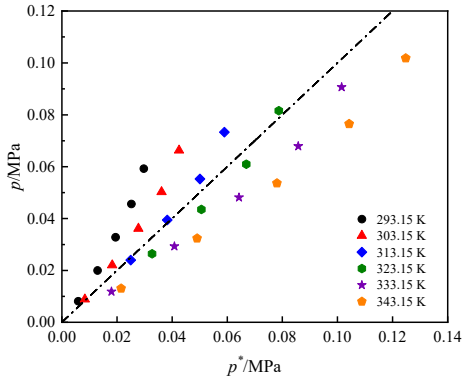

Figure 8. Deviation of R1336mzz(Z)/DiPEC7 system from Raoult's law.

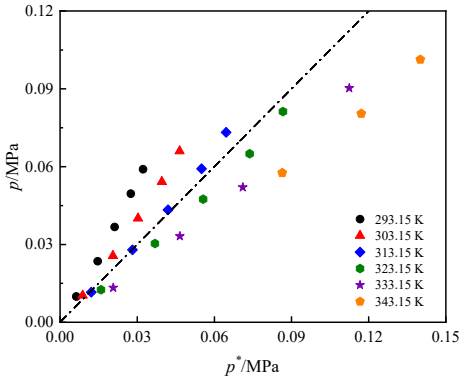

Figure 9. Deviation of R1336mzz(Z)/DiPEiC9 system from Raoult's law.

3.2. Solubility Comparison

The Henry's constant (*He*) can reflect the dissolution potential of a solute in a solvent [35]. The calculation formula for *He* is as follows [36]:

$$He = \lim_{x_1 \to 0} \left[\gamma_1 p_1^s \exp\left(\frac{\left(B_{11} - 1/\rho_{1,\text{liquid}}^1 \right) p_1^s}{RT} \right) \right] \tag{17}$$

Figure 10 compares the Henry's constants of R1336mzz(Z)/DiPEC7 and R1336mzz(Z)/-DiPEiC9 mixtures within the temperature range of 293.15 K–343.15 K. The results show that when the temperature is lower than 328.15 K, the *He* of R1336mzz(Z)/DiPEC7 is smaller than that of R1336mzz(Z)/DiPEiC9. However, when the temperature is higher than 328.15 K, the *He* of R1336mzz(Z)/DiPEC7 is larger than that of R1336mzz(Z)/DiPEiC9. This indicates that the R1336mzz(Z)/DiPEiC9 system is less sensitive to temperature. The reason may lie in the branched-chain structure of DiPEiC9, as indicated in Figure 3. The three-dimensional structure formed by the branched chains provides a relatively fixed accommodation space for refrigerant molecules, preventing them from easily detaching due to thermal motion and weakening the influence of temperature on solubility.

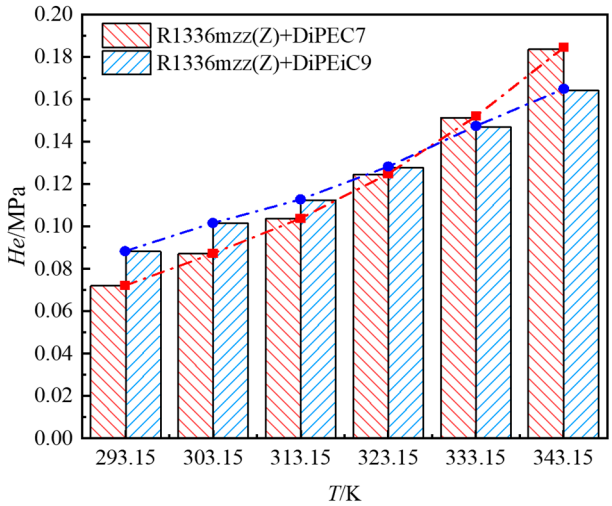

Figure 10. Comparison of the Henry's constants of R1336mzz(Z)/DiPEC7 and R1336mzz(Z)/-DiPEiC9 systems.

Figure 11 shows the comparison of the solubilities of R1336mzz(Z) in DiPEC7, DiPEiC9, and POE SE220 at 333.15 K [23]. The solubility of R1336mzz(Z) in dipentaerythritol esters is higher than that in the commercial POE SE220 oil. Due to the complex composition of POE oils, each pure component can affect the solubility of R1336mzz(Z). Therefore, a

comprehensive and systematic investigation on the solubility behavior of R1336mzz(Z) in the individual pure components of POE oils is essential.

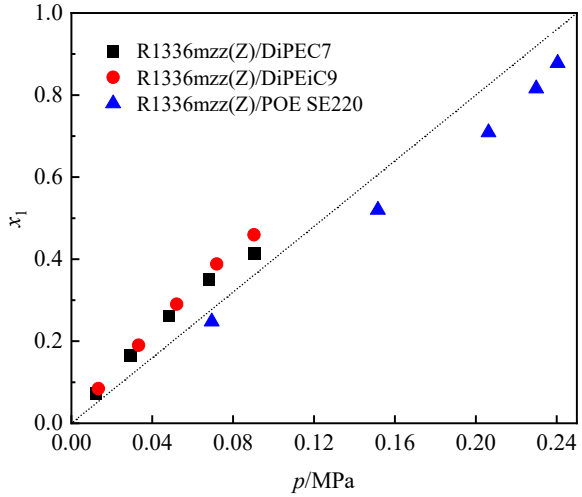

Figure 11. Comparison of the solubilities of R1336mzz(Z) in DiPEC7, DiPEiC9, and POE SE220 at 333.15 K [23].

3.3. Mixing Thermodynamic Properties

Studying the dissolution behavior of R1336mzz(Z) in DiPECs allows for better understanding the intermolecular interactions. In this work, the mixing thermodynamic properties including the enthalpy change ΔH_{mix}, entropy change ΔS_{mix}, and Gibbs free energy change ΔG_{mix} in the mixing process were calculated based on the solubility data. The calculated formulas are follows [37]:

$$\Delta H_{mix} = \Delta H^{id} + H^{E} \tag{18}$$

$$\Delta S_{mix} = \Delta S^{id} + S^{E} \tag{19}$$

$$\Delta G_{mix} = \Delta G^{id} + G^{E} \tag{20}$$

For an ideal solution, $\Delta H^{id} = 0$. ΔS^{id}, ΔG^{id}, H^{E}, S^{E}, and G^{E} are calculated by:

$$\Delta S^{id} = -R\sum_{i} x_i \ln x_i = -R(x_1 \ln x_1 + x_2 \ln x_2) \tag{21}$$

$$\Delta G^{id} = RT\sum_{i} x_i \ln x_i = RT(x_1 \ln x_1 + x_2 \ln x_2) \tag{22}$$

$$H^{E} = -RT^2\left[x_1 \frac{\partial(\ln \gamma_1)}{\partial T} + x_2 \frac{\partial(\ln \gamma_2)}{\partial T}\right] \tag{23}$$

$$S^{E} = \frac{H^{E} - G^{E}}{T} \tag{24}$$

$$G^{E} = RT\sum_{i} x_i \ln \gamma_i = RT(x_1 \ln \gamma_1 + x_2 \ln \gamma_2) \tag{25}$$

In Equations (18) to (25), the superscripts "id" and "E" mean the ideal solution and the excess properties of the mixtures. The calculated results of ΔH_{mix}, ΔS_{mix}, and ΔG_{mix} for R1336mzz(Z)/DiPEC7 and R1336mzz(Z)/DiPEiC9 are presented in Tables 6 and 7, respectively. Both the mixing enthalpy change and mixing entropy change are positive, which proves that the dissolution process is an exothermic and irreversible process. In addition, the change in Gibbs free energy during the mixing process is negative, which is consistent with general thermodynamic laws.

Table 6. The mixing enthalpy, entropy, and Gibbs free energy of R1336mzz(Z) dissolving in DiPEC7.

T (K)	x_1	ΔH_{mix} (J·mol^{-1})	ΔS_{mix} (J·mol^{-1}·K^{-1})	ΔG_{mix} (J·mol^{-1})
293.15	0.099	1351.05	7.05	−714.70
293.15	0.215	3090.70	14.23	−1079.48
293.15	0.324	4854.82	20.65	−1198.80
293.15	0.419	6494.43	26.13	−1164.56
293.15	0.494	7836.38	30.33	−1054.97
303.15	0.093	1387.28	7.08	−760.49
303.15	0.205	3152.40	14.36	−1200.81
303.15	0.311	4945.46	20.94	−1401.67
303.15	0.406	6623.76	26.60	−1440.40
303.15	0.477	7927.58	30.74	−1391.36
313.15	0.195	2615.67	12.52	−1305.82
313.15	0.299	4103.34	18.15	−1580.41
313.15	0.391	5491.69	22.93	−1688.02
313.15	0.461	6570.35	26.39	−1692.17
323.15	0.183	782.05	4.85	−1369.67
323.15	0.283	2920.31	14.32	−1707.72
323.15	0.374	3907.61	17.90	−1876.84
323.15	0.440	4636.07	20.31	−1926.24
333.15	0.074	565.17	4.08	−795.70
333.15	0.167	1268.71	7.96	−1384.44
333.15	0.263	1973.29	11.26	−1776.79
333.15	0.351	2604.05	13.81	−1998.38
333.15	0.415	3056.67	15.44	−2087.74
343.15	0.066	457.35	3.57	−768.60
343.15	0.150	999.06	6.89	−1365.10
343.15	0.238	1513.76	9.64	−1792.98
343.15	0.318	1929.18	11.60	−2052.46
343.15	0.381	2221.33	12.84	−2183.77

Table 7. The mixing enthalpy, entropy, and Gibbs free energy of R1336mzz(Z) dissolving in DiPEiC9.

T (K)	x_1	ΔH_{mix} (J·mol^{-1})	ΔS_{mix} (J·mol^{-1}·K^{-1})	ΔG_{mix} (J·mol^{-1})
293.15	0.105	1564.06	7.73	−701.76
293.15	0.243	3677.08	16.15	−1057.84
293.15	0.353	5418.21	22.35	−1132.62
293.15	0.457	7105.54	27.89	−1069.34
293.15	0.536	8410.79	31.90	−940.54
303.15	0.099	2036.09	9.23	−760.53
303.15	0.231	4743.18	19.68	−1222.57
303.15	0.340	6955.06	27.52	−1387.48
303.15	0.444	9043.68	34.47	−1404.86
303.15	0.521	10582.22	39.32	−1336.88
313.15	0.095	1731.47	8.17	−827.96
313.15	0.220	3904.71	16.87	−1377.41
313.15	0.328	5692.07	23.39	−1631.97
313.15	0.430	7291.74	28.80	−1727.94
313.15	0.504	8412.21	32.35	−1718.08
323.15	0.089	1262.21	6.58	−863.68
323.15	0.206	2746.49	13.07	−1477.49
323.15	0.311	3899.37	17.64	−1801.77
323.15	0.412	4858.54	21.11	−1963.76
323.15	0.484	5450.15	23.05	−1997.78
333.15	0.085	1111.99	6.02	−893.60
333.15	0.190	2277.23	11.43	−1529.48
333.15	0.290	3142.57	15.16	−1909.42
333.15	0.460	4080.98	18.84	−2195.77
343.15	0.264	3323.86	15.43	−1972.47
343.15	0.358	3973.34	18.13	−2246.47
343.15	0.428	4272.83	19.33	−2359.05

4. Conclusions

To address the lack of solubility data for R1336mzz(Z) in POE lubricants, the solubilities of R1336mzz(Z) in DiPEC7 and DiPEiC9 were reported within the temperature range of 293.15 K–343.15 K in this work. The solubility data were correlated using the NRTL model. The AARD between the experimental mole fractions and calculated values from the NRTL

model are 1.88% and 1.46% for the R1336mzz(Z)/DiPEC7 and R1336mzz(Z)/DiPEiC9 mixtures, respectively. In addition, the deviation between the mixtures and the ideal system was calculated according to Raoult's law. The calculated results show that as temperature increases, the deviation of the binary mixtures from Raoult's law gradually shifts from positive to negative. This phenomenon indicates that with increasing temperature, the intermolecular forces between the refrigerant and lubricant molecules gradually become stronger than those among refrigerant molecules. Furthermore, by calculating the Henry's constants (*He*), the dissolution potential of R1336mzz(Z) in DiPEC7 and DiPEiC9 was compared. The results show that for temperatures below 328.15 K, the *He* of R1336mzz(Z) in DiPEC7 is lower than that in DiPEiC9; conversely, at temperatures exceeding 328.15 K, the *He* of R1336mzz(Z) in DiPEC7 becomes higher than that in DiPEiC9. The mixing thermodynamic properties of R1336mzz(Z) dissolving in DiPECs, such as the mixing enthalpy change, mixing entropy change, and mixing Gibbs free energy change, were analyzed. The mixing enthalpy change and mixing entropy change are positive, indicating that the dissolution process is an exothermic and irreversible process.

Author Contributions: C.L.: writing—resources, data curation, formal analysis, methodology, and original draft. W.D.—visualization and validation. X.W.—project administration, conceptualization, and review and editing. All authors have read and agreed to the published version of the manuscript.

Funding: This research is supported by the National Key Research and Development Program of China (Grant No. 2022YFE0210200).

Data Availability Statement: All data are available from the corresponding author by request.

Conflicts of Interest: The authors declare no conflicts of interest.

References

1. Vuppaladadiyam, A.K.; Antunes, E.; Vuppaladadiyam, S.S.V.; Baig, Z.T.; Subiantoro, A.; Lei, G.Y.; Leu, S.Y.; Sarmah, A.K.; Duan, H.B. Progress in the development and use of refrigerants and unintended environmental consequences. *Sci. Total Environ.* **2022**, *823*, 153670. [CrossRef]
2. Perry, C.; Nickson, T.; Starr, C.; Grabiel, T.; Geoghegan, S.; Porter, B.; Mahapatra, A.; Walravens, F. More to offer from the Montreal protocol: How the ozone treaty can secure further significant greenhouse gas emission reductions in the future. *J. Integr. Environ. Sci.* **2024**, *21*, 2362124. [CrossRef]
3. Liu, H.P.; Duan, H.B.; Zhang, N.; Ma, Y.; Liu, G.; Miller, T.R.; Mao, R.C.; Xu, M.; Li, J.H.; Yang, J.K. Rethinking time-lagged emissions and abatement potential of fluorocarbons in the post-Kigali Amendment era. *Nat. Commun.* **2024**, *15*, 6687. [CrossRef]
4. Heath, E.A. Amendment to the Montreal Protocol on substances that deplete the ozone layer (Kigali Amendment). *Int. Leg. Mater.* **2017**, *56*, 193–205. [CrossRef]
5. Nair, V. HFO refrigerants: A review of present status and future prospects. *Int. J. Refrig.* **2021**, *122*, 156–170. [CrossRef]
6. Molés, F.; Navarro-Esbrí, J.; Peris, B.; Mota-Babiloni, A.; Barragán-Cervera, Á.; Kontomaris, K. Low GWP alternatives to HFC-245fa in Organic Rankine Cycles for low temperature heat recovery: HCFO-1233zd-E and HFO-1336mzz-Z. *Appl. Therm. Eng.* **2014**, *71*, 204–212. [CrossRef]
7. Tanaka, K.; Akasaka, R.; Sakaue, E.; Ishikawa, J.; Kontomaris, K.K. Measurements of the critical parameters for cis-1,1,1,4,4,4-Hexafluoro-2-butene. *J. Chem. Eng. Data* **2017**, *62*, 1135–1138. [CrossRef]
8. Arpagaus, C.; Bless, F.; Uhlmann, M.; Schiffmann, J.; Bertsch, S.S. High temperature heat pumps: Market overview, state of the art, research status, refrigerants, and application potentials. *Energy* **2018**, *152*, 985–1010. [CrossRef]
9. Sakoda, N.; Higashi, Y.; Akasaka, R. Measurements of vapor pressures for trans-1-Chloro-3,3,3-trifluoropropene (R1233zd(E)) and cis-1,1,1,4,4,4-hexafluoro-2-butene (R1336mzz(Z)). *J. Chem. Eng. Data* **2020**, *65*, 4285–4289. [CrossRef]
10. Kano, Y. Thermophysical properties evaluation for a polar fluid on the basis of the experimentally determined heat capacity and dipole moment in the ideal gas states. *J. Therm. Anal. Calorim.* **2023**, *148*, 5573–5587. [CrossRef]
11. Alam, M.J.; Miyara, A.; Kariya, K.; Kontomaris, K.K. Measurement of viscosity of cis-1,1,1,4,4,4-Hexafluoro-2-butene (R-1336mzz(Z)) by Tandem capillary tubes method. *J. Chem. Eng. Data* **2018**, *63*, 1706–1712. [CrossRef]
12. Alam, M.J.; Islam, M.A.; Kariya, K.; Miyara, A. Measurement of thermal conductivity of cis-1,1,1,4,4,4-hexafluoro-2-butene (R-1336mzz(Z)) by the transient hot-wire method. *Int. J. Refrig.* **2017**, *84*, 220–227. [CrossRef]

13. Perkins, R.A.; Huber, M.L. Measurement and correlation of the thermal conductivity of cis-1,1,1,4,4,4-hexafluoro-2-butene. *Int. J. Thermophys.* **2020**, *41*, 103. [CrossRef]
14. Tijani, M.E.H.; Otero Rodriguez, G.J.; Ramirez, M.; Poulsen, J.L.; Spoelstra, S. Selection of lubricant oils for high temperature heat pumps: A review and selection methodology guidelines. *Appl. Therm. Eng.* **2025**, *273*, 126483. [CrossRef]
15. García, J.; Abou Naccoul, R.; Fernández, J.; Razzouk, A.; Mokbel, I. Vapor-pressure measurements and modeling of dipentaerythritol ester lubricants. *Ind. Eng. Chem. Res.* **2011**, *50*, 4231–4237. [CrossRef]
16. Emel'ianov, V.V.; Krasnykh, E.L.; Sokolov, A.B. Synthetic oils based on pentaerythritol esters. Kinematic viscosity. *Fluid Phase Equilib.* **2024**, *581*, 114074. [CrossRef]
17. Paredes, X.; Pensado, A.S.; Comuñas, M.J.P.; Fernández, J. Experimental dynamic viscosities of dipentaerythritol ester lubricants at high pressure. *J. Chem. Eng. Data* **2010**, *55*, 3216–3223. [CrossRef]
18. Harris, K.R. Temperature and pressure dependence of the viscosities of Krytox GPL102 Oil and di(pentaerythritol) hexa(isononanoate). *J. Chem. Eng. Data* **2015**, *60*, 1510–1519. [CrossRef]
19. Lu, C.; Zhang, Y.J.; Wang, X.P. Density, viscosity, and R1234yf solubility in dipentaerythritol esters. *J. Chem. Eng. Data* **2025**, *70*, 2057–2067. [CrossRef]
20. Morales-Espejel, G.E.; Wallin, H.H.; Hauleitner, R.; Arvidsson, M. Progress in rolling bearing technology for refrigerant compressors. *Proc. Inst. Mech. Eng. Part C-J. Mech. Eng. Sci.* **2017**, *232*, 2948–2961. [CrossRef]
21. Sun, Y.J.; Wang, X.D.; Wang, S.B.; Meng, X.Z. Viscosity measurement and correlation of saturated solutions of R-290 with three lubricants. *Int. J. Refrig.* **2023**, *155*, 1–6. [CrossRef]
22. Wang, C.C.; Hafner, A.; Kuo, C.S.; Hsieh, W.D. An overview of the effect of lubricant on the heat transfer performance on conventional refrigerants and natural refrigerant R-744. *Renew. Sustain. Energy Rev.* **2012**, *16*, 5071–5086. [CrossRef]
23. Brocus, J.; Valtz, A.; Coquelet, C.; De Carlan, F. Solubility measurements of refrigerants in polyolesters lubricants at temperature from 323 K to 383 K. *Int. J. Refrig.* **2022**, *134*, 278–292. [CrossRef]
24. Luo, Y.; Liu, Z.; Lu, C.; Wang, X.P. Vapor-liquid equilibrium measurements of 3, 3, 3-trifluoropropene with pentaerythritol tetraheptanoate and pentaerythritol tetranonanoate. *J. Chem. Thermodyn.* **2022**, *174*, 106874. [CrossRef]
25. Lu, C.; Zhang, Y.J.; Wang, X.P. Solubility measurements of R1234ze(E), R1243zf, and R1234yf in POE46 at temperatures from 283.15 to 343.15 K. *J. Chem. Eng. Data* **2024**, *69*, 1677–1684. [CrossRef]
26. Sun, Y.J.; Li, X.J.; Meng, X.Y.; Wu, J.T. Measurement and correlation of the liquid density and viscosity of HFO-1336mzz(Z) (cis-1,1,1,4,4,4-hexafluoro-2-butene) at high pressure. *J. Chem. Eng. Data* **2019**, *64*, 395–403. [CrossRef]
27. Bich, W.; Cox, M.G.; Dybkaer, R.; Elster, C.; Estler, W.T.; Hibbert, B.; Imai, H.; Kool, W.; Michotte, C.; Nielsen, L.; et al. Revision of the 'Guide to the Expression of Uncertainty in Measurement'. *Metrologia* **2012**, *49*, 702. [CrossRef]
28. Goharshadi, E.K.; Moosavi, M.; Abareshi, M. Calculation of thermodynamic properties of lubricant + refrigerant mixtures using GMA equation of state. *Int. J. Therm. Sci.* **2007**, *46*, 944–952. [CrossRef]
29. Comuñas, M.J.P.; Baylaucq, A.; Boned, C.; Canet, X.; Fernández, J. High-pressure volumetric behavior of x 1,1,1,2-tetrafluoroethane + (1 − x) 2,5,8,11,14-pentaoxapentadecane (TEGDME) mixtures. *J. Chem. Eng. Data* **2002**, *47*, 233–238. [CrossRef]
30. Saggion, A.; Faraldo, R.; Pierno, M. *Thermodynamics: Fundamental Principles and Applications*; Springer: Cham, Switzerland, 2019.
31. Beattie, J.A.; Stockmayer, W.H. The Second Virial Coefficient for Gas Mixtures. *J. Chem. Phys.* **1942**, *10*, 473–476. [CrossRef]
32. Lemmon, E.W.; Bell, I.H.; Huber, M.L.; McLinden, M.O. *NIST Standard Reference Database 23: Reference Fluid Thermo-Dynamic and Transport Properties-REFPROP, Version 10.0.*; National Institute of Standards and Technology: Gaithersburg, MD, USA, 2019.
33. Renon, H.; Prausnitz, J.M. Local compositions in thermodynamic excess functions for liquid mixtures. *AIChE J.* **2004**, *14*, 135–144. [CrossRef]
34. Masuku, C.M.; Ma, W.; Hildebrandt, D.; Glasser, D.; Davis, B.H. A vapor–liquid equilibrium thermodynamic model for a Fischer–Tropsch reactor. *Fluid Phase Equilibr.* **2012**, *314*, 38–45. [CrossRef]
35. Gunn, R.D.; Yamada, T.; Whitman, D. Corresponding states. III. Henry'constants for nonpolar binary mixtures. *AIChE J.* **1974**, *20*, 906–915. [CrossRef]
36. Sun, Y.J.; Di, G.L.; Wang, J.; Wang, X.P.; He, M.G. Phase behavior of R1234yf and R600a in pentaerythritol tetranonanoate. *Int. J. Refrig.* **2020**, *109*, 135–142. [CrossRef]
37. Prausnitz, J.M.; Lichtenthaler, R.N.; de Azevedo, E.G. *Molecular Thermodynamics of Fluid Phase Equilibria*, 3rd ed.; Prentice Hall PTR: Hoboken, NJ, USA, 1999.

Disclaimer/Publisher's Note: The statements, opinions and data contained in all publications are solely those of the individual author(s) and contributor(s) and not of MDPI and/or the editor(s). MDPI and/or the editor(s) disclaim responsibility for any injury to people or property resulting from any ideas, methods, instructions or products referred to in the content.